A fast integral equation based scheme for computing magneto-static fields in nonlinear media

by

Sridharan Balasubramanian

A thesis submitted to the graduate faculty

in partial fulfillment of the requirements for the degree of

MASTER OF SCIENCE

Major: Electrical Engineering

Major Professor: Shanker Balasubramaniam

Iowa State University

Ames, Iowa

2001

Graduate College
Iowa State University

This is to certify that the Master's thesis of

Sridharan Balasubramanian

has met the thesis requirements of Iowa State University

Signatures have been redacted for privacy

TABLE OF CONTENTS

LIST OF FIGURES

ABSTRACT

Large scale magneto-static field analysis in both the linear and non-linear regime are typically performed using differential equation (DE) based schemes; integral equation (IE) based schemes are less popular. This is in large part due to the computational complexity and memory requirements associated with IE-based schemes, both of which scale as $\mathcal{O}(N^2)$ where N is the total number of unknowns used for the analysis. Reducing this complexity has been a focus of considerable research. In this thesis, we introduce a novel IE that is cast in terms of the magnetic flux density. This enables us to construct a solution using the method of moments (MoM) by choosing vector basis functions that satisfy the requisite boundary condition. This solver is then augmented with a recently introduced version of the fast multipole method. The magnetic field distributions computed using this scheme are validated against those obtained analytically. Finally, the efficacy of this scheme is demonstrated by applying it to the analysis of practical problems where the permeability is non-linear.

CHAPTER 1. INTRODUCTION

1.1 Literature Review

Evaluating magnetic field distribution is crucial for numerous practical applications. For instance, magnetic particle inspection (3; 38), magnetic flux leakage (24) and the analysis and design of the magnetic shielding (17), benefit from the availability of robust schemes for evaluating magneto-static fields in inhomogeneous domains. Furthermore, in many practical applications, the field intensity is sufficiently high that the non-linear behavior of the permeability should be rigorously included in the analysis. Typically, magneto-static fields in inhomogeneous media are analyzed using either a differential equation (DE)- (29) or an integral equation (IE)-based methods (37). Common differential equation based techniques like the finite difference method and the finite element method demand the presence of perfectly matched layers to truncate the boundary and, therefore are not efficient in solving open boundary problems (43; 10; 42). In contrast, the Green's functions used in the integral equation based techniques implicitly account for the boundary conditions (20; 41). Typically, integral equation based schemes give rise to dense matrices, whose inversion is expensive. Indeed, if the object being analyzed is discretized using N unknowns, both the memory and the computational complexity scale as $\mathcal{O}(N^2)$. The demand on computational resources seems to be the chief obstacle in preventing the widespread use of IE-based schemes. Reducing this complexity, thus, has been the focus of intense research over the past decade. The fast multipole method introduced by Rokhlin (8) successfully addresses most of these problems. Indeed, fast multipole augmented IE-based schemes have been used for a vast variety of applications ranging from capacitance extraction and molecular dynamics to large scale simulations in astrophysics (25; 2; 14).

Magnetic field distribution in non-linear media is typically analyzed using volume inte-

gral equations. These can be reduced to surface integral equations provided the material is homogeneous, and the field intensity is such that the permeability can be approximated as being constant. In the early 1970s, one of the first volume integral equations for nonlinear magnetostatics (GFUN code, see (27)) was developed. GFUN is based on a piecewise constant vector approximation of magnetic field strength **H** inside elements. In the last two decades, most of the analysis relied on scalar formulations; see (38; 18; 34; 19) and references therein. Recently, Kettunen *et al.* (16) introduced a h-field formulation and demonstrated its accuracy and efficiency in a high performance computing environment. In this thesis, we introduce an IE that is based on the magnetic flux density. This equation is solved using vector basis functions that impose normal continuity of the fields (36). The IE, then, is validated by comparing the field distribution in a spherical shell with a constant permeability obtained numerically against analytical results.

1.2 Organization

This thesis is organized as follows: Chapter 2 outlines the volume integral equation for the magneto-static problem and its conversion to a matrix equation using the method of moments (MoM). Chapter 3, briefly describes the FMM and its incorporation into the solution procedure. A plethora of numerical results are presented in Chapter 4. These serve to demonstrate the accuracy of our scheme and its applicability to the analysis of large practical problems. Finally, Chapter 5 summarizes the contribution of this work.

CHAPTER 2. FORMULATION OF THE INTEGRAL EQUATION

2.1 Description of the problem

Consider an inhomogeneous body with nonlinear magnetic permeability $\mu(\mathbf{r})$ occupying a volume V in free space and bounded by a surface S (see Figure 2.1). The body is assumed to be isotropic and is immersed in an ambient magnetic field $\mathbf{H}^i(\mathbf{r})$.

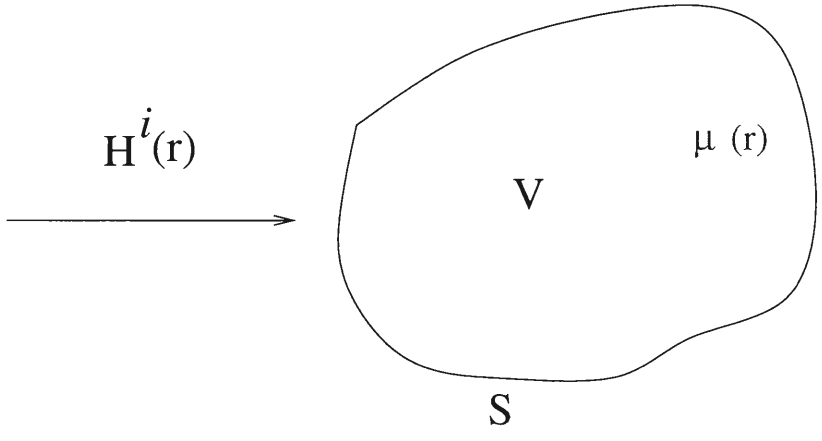

Figure 2.1 Inhomogeneous body immersed in an ambient magnetic field.

The presence of the body perturbs the field and the total magnetic field can be written as:

$$\mathbf{H}^t(\mathbf{r}) = \mathbf{H}^i(\mathbf{r}) + \mathbf{H}^p(\mathbf{r}). \tag{2.1}$$

The perturbed magnetic field, $\mathbf{H}^p(\mathbf{r})$, is fully characterized by the magnetic scalar potential due to the body and is expressed as $\mathbf{H}^p(\mathbf{r}) = -\nabla\phi^p(\mathbf{r})$.

2.2 Formulation of the Integral Equation

This magnetic field induces a magnetization current density $\mathbf{M}(\mathbf{r})$ in the body that in turn creates a magnetic field $\mathbf{H}^p(\mathbf{r})$. This field can be related to the magnetic scalar potential $\phi^p(\mathbf{r})$ (31) as follows:

$$\mathbf{H}^p(\mathbf{r}) = -\nabla\phi^p(\mathbf{r}); \phi^p(\mathbf{r}) = \frac{1}{4\pi}\int_S \frac{\mathbf{M}(\mathbf{r}')\cdot\hat{\mathbf{n}}}{R}ds' - \frac{1}{4\pi}\int_V \frac{\nabla'\cdot\mathbf{M}(\mathbf{r}')}{R}dv' \tag{2.2}$$

In the above equation, $R = |\mathbf{r} - \mathbf{r}'|$ denotes the distance between the source and the observer points, and $\hat{n}$ is the outward normal at any point on the surface S. The quantities $\mathbf{M}(\mathbf{r}')\cdot\hat{\mathbf{n}}$ and $\nabla\cdot\mathbf{M}(\mathbf{r}')$ may be interpreted as the equivalent surface and volume magnetic charge densities, respectively. The magnetization current density is related to the total magnetic field via $\mathbf{M}(\mathbf{r}) = \chi\left(|\mathbf{H}^t(\mathbf{r})|\right)\mathbf{H}^t(\mathbf{r})$ where $\chi\left(|\mathbf{H}^t(\mathbf{r})|\right) = \mu_r\left(|\mathbf{H}^t(\mathbf{r})|\right) - 1$ is the susceptibility and $\mu_r\left(|\mathbf{H}^t(\mathbf{r})|\right)$ is the relative permeability of the material and $\mathbf{H}^t(\mathbf{r})$ is the total magnetic field. Denoting $\phi^t(\mathbf{r})$ and $\phi^i(\mathbf{r})$ as the total and incident magnetic scalar potential, respectively, and using $\mathbf{H}^t(\mathbf{r}) = -\nabla\phi^t(\mathbf{r}), \mathbf{H}^i(\mathbf{r}) = -\nabla\phi^i(\mathbf{r})$ together with Equation (2.2) results in an integral equation in terms of the scalar potential:

$$\phi^t(\mathbf{r}) = \phi^i(\mathbf{r}) - \frac{1}{4\pi}\int_S \frac{\chi\left(|\mathbf{H}^t(\mathbf{r}')|\right)\nabla'\phi^t(\mathbf{r}')\cdot\hat{\mathbf{n}}}{R}ds' + \frac{1}{4\pi}\int_V \frac{\nabla'\cdot\left(\chi\left(|\mathbf{H}^t(\mathbf{r}')|\right)\nabla'\phi^t(\mathbf{r}')\right)}{R}dv'. \tag{2.3}$$

As is apparent from the above equation, the nonlinearity of the material has been embedded in the magnetic susceptibility. It can be verified that the above equation reduces to

$$\phi^t(\mathbf{r}) = \phi^i(\mathbf{r}) - \frac{1}{4\pi}\int_V \chi\left(|\mathbf{H}^t(\mathbf{r}')|\right)\nabla'\phi^t(\mathbf{r}')\cdot\frac{\hat{\mathbf{R}}}{R^2}dv' \tag{2.4}$$

as in (10).

In what follows, it will be implicitly assumed that the constitutive parameters are nonlinear and will be suppressed. The integral equation described in (2.3) or in (2.4) can be discretized using scalar basis functions (10) and solved using the method of moments (MoM) (11). However, as opposed to the method prescribed in (10), we cast the integral equation in a slightly different form that enables us to choose appropriate basis functions that represent physical

quantities of interest as well as permit the application of the FMM to accelerate the solution procedure. Observe that taking the gradient of the Equation 2.3 results in

$$\nabla\phi^t(\mathbf{r}) = -\mathbf{H}^i(\mathbf{r}) - \frac{1}{4\pi}\nabla\int_S \frac{\chi(\mathbf{r}')\nabla'\phi^t(\mathbf{r}')\cdot\hat{\mathbf{n}}}{R}ds' + \frac{1}{4\pi}\nabla\int_V \frac{\nabla'\cdot(\chi(\mathbf{r}')\nabla'\phi^t(\mathbf{r}'))}{R}dv'. \quad (2.5)$$

Before embarking on the description of the MoM scheme, note that the quantity $-\mu(\mathbf{r})\nabla\phi^t(\mathbf{r})$ is the total magnetic flux density. Thus, Equation 2.5 reduces to finding the distribution of the magnetic flux density, $\mathbf{B}(\mathbf{r})$ throughout the body and can be rewritten as

$$\frac{\mathbf{B}(\mathbf{r})}{\mu(\mathbf{r})} = \mathbf{H}^i(\mathbf{r}) - \frac{1}{4\pi}\nabla\int_S \frac{\chi(\mathbf{r}')\mathbf{B}(\mathbf{r}')}{\mu(\mathbf{r}')R}\cdot\hat{\mathbf{n}}ds' + \frac{1}{4\pi}\nabla\int_V \frac{1}{R}\,\nabla'\cdot\frac{\chi(\mathbf{r}')\mathbf{B}(\mathbf{r}')}{\mu(\mathbf{r}')}dv'. \quad (2.6)$$

2.3 Solution Procedure

2.3.1 Basis Functions

In what follows, we shall prescribe a procedure to efficiently solve the above integro-differential equation. Pursuant to this objective, the flux density is represented using basis functions, introduced by Schaubert *et al* (36) to compute scattering from dielectric obstacles. These basis functions can be thought of as the three dimensional analogue of rooftop basis functions (30). These basis functions are defined on a pair of tetrahedra and preserve normal continuity of the flux density. Consequently, the spatial variation of the flux density may be represented using

$$\mathbf{B}(\mathbf{r}) = \sum_{n=1}^{N} B_n\mathbf{f}_n(\mathbf{r}) \quad (2.7)$$

where N is the number of unknowns and B_n is the unknown expansion coefficient.

The spatial basis (see Figure (2.2)) functions associated with the n^{th} face are defined as:

$$\mathbf{f}_n(\mathbf{r}) = \begin{cases} \dfrac{a_n}{3v_n^+}\boldsymbol{\rho}_n^+ & \mathbf{r}\in T_n^+ \\ \dfrac{a_n}{3v_n^-}\boldsymbol{\rho}_n^- & \mathbf{r}\in T_n^- \end{cases} \quad (2.8)$$

where $T_n^\pm$ are the pair of tetrahedra that share the n^{th} face , a_n is the area of n^{th} face, and $v_n^\pm$ is the volume of $T_n^\pm$. The vector $\boldsymbol{\rho}_n^+$ is defined from the free vertex of T_n^+ to the position vector $\mathbf{r}$; $\boldsymbol{\rho}_n^-$ is defined similarly except that it is directed towards the free vertex of T_n^-. The

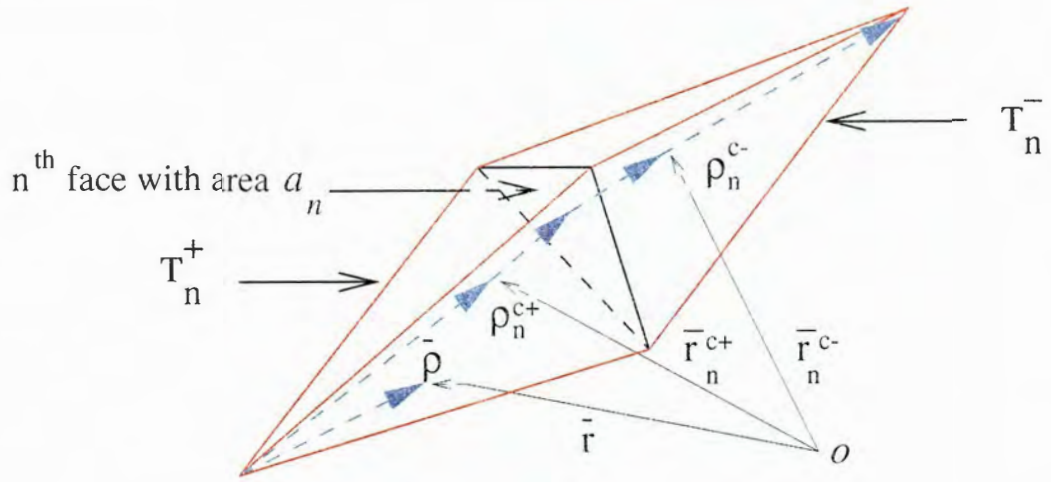

Figure 2.2 Geometrical Parameters associated with the n^{th} face.

subscripts refer to faces and the superscripts refer to tetrahedra. The triangular faces residing on the boundary of V have basis functions that are non-zero over a single tetrahedron since only one of it is associated with those faces.

2.3.2 Matrix Equations

The integral equation is now discretized using a Galerkin testing procedure. Upon substitution of the magnetic flux density representation given by Equation (2.7) into Equation (2.6), the resulting equation is tested with the basis functions $\mathbf{f}_m(\mathbf{r}), m = 1, ..., N$, using the symmetric inner product, $< \mathbf{f}_m(\mathbf{r}), \mathbf{g}_m(\mathbf{r}) > = \int_V \mathbf{f}_m(\mathbf{r}) \cdot \mathbf{g}_m(\mathbf{r}) dv$. After testing, the final equation can be written as:

$$< \mathbf{f}_m(\mathbf{r}), \frac{\mathbf{B}(\mathbf{r})}{\mu(\mathbf{r})} > + < \mathbf{f}_m(\mathbf{r}), \nabla\phi^p(\mathbf{r}) > = < \mathbf{f}_m(\mathbf{r}), \mathbf{H}^i(\mathbf{r}) > \tag{2.9}$$

This represents N independent equations for the unknown expansion coefficients $\{B_n\}$. In matrix form this yields

$$\mathcal{Z}\,\mathcal{B} = \mathcal{H} \tag{2.10a}$$

where $\mathcal{B}$ is an array of weights $[B_1, B_2, \cdots, B_N]^T$ and $\mathcal{H} = [H_1, H_2, \cdots, H_N]^T$ is evaluated as

$$\mathcal{H}_m = \frac{a_m}{3}\left[\frac{1}{v_m^+}\int_{T_m^+} \mathbf{H}^i(\mathbf{r}) \cdot \boldsymbol{\rho}_m^+ dv + \frac{1}{v_m^-}\int_{T_m^-} \mathbf{H}^i(\mathbf{r}) \cdot \boldsymbol{\rho}_m^- dv\right]. \tag{2.10b}$$

$\mathcal{Z}$ is the interaction matrix. Each element of the interaction matrix is given by

$$Z_{mn} =< \mathbf{f}_m(\mathbf{r}), \frac{\mathbf{f}_n(\mathbf{r})}{\mu(\mathbf{r})} > + < \mathbf{f}_m(\mathbf{r}), \nabla\phi_n^p(\mathbf{r}) > \tag{2.10c}$$

where the self contribution ($Z_{mn}^{self} = < \mathbf{f}_m(\mathbf{r}), \frac{\mathbf{f}_n(\mathbf{r})}{\mu(\mathbf{r})} >$) to Z_{mn} is evaluated as

$$Z_{mn}^{self} = \left[\frac{1}{\mu_m^+}\int_{T_m^+} \mathbf{f}_m(\mathbf{r})\cdot\mathbf{f}_n(\mathbf{r})dv + \frac{1}{\mu_m^-}\int_{T_m^-} \mathbf{f}_m(\mathbf{r})\cdot\mathbf{f}_n(\mathbf{r})dv\right] \tag{2.11}$$

where $\mu_m^{\pm}$ is the permeability within $T_m^{\pm}$ and the integrals are evaluated analytically using (36). Finally, the second term on the right hand side of Equation (2.10c), denoted as Z_{mn}^{ϕ}, can be expanded as

$$Z_{mn}^{\phi} = < \mathbf{f}_m(\mathbf{r}), \nabla\phi_n^p(\mathbf{r}) > = \int_S \phi_n^p(\mathbf{r})\mathbf{f}_m(\mathbf{r})\cdot\hat{\mathbf{n}}ds - \int_V \phi_n^p(\mathbf{r})\nabla\cdot\mathbf{f}_m(\mathbf{r})dv \tag{2.12}$$

and is evaluated using a procedure similar to that given in (36) as:

$$Z_{mn}^{\phi} = \begin{cases} +a_m\left[\frac{1}{v_m^-}\int_{T_m^-}\phi_n^p(\mathbf{r})dv - \frac{1}{v_m^+}\int_{T_m^+}\phi_n^p(\mathbf{r})dv\right] & T_m^+ \text{ and } T_m^- \in V \\ \pm a_m\left[\frac{1}{a_m}\int_{a_m}\phi_n^p(\mathbf{r})dS - \frac{1}{v_m^{\pm}}\int_{T_m^{\pm}}\phi_n^p(\mathbf{r})dv\right] & T_m^{\mp} \notin V \end{cases} \tag{2.13}$$

where

$$\phi_n^p(\mathbf{r}) = \frac{1}{4\pi}\int_S \frac{\chi(\mathbf{r}')\mathbf{f}_n(\mathbf{r}')}{\mu(\mathbf{r}')R}\cdot\hat{\mathbf{n}}\,ds' - \frac{1}{4\pi}\int_V \frac{1}{R}\,\nabla'\cdot\frac{\chi(\mathbf{r}')\mathbf{f}_n(\mathbf{r}')}{\mu(\mathbf{r}')}dv'. \tag{2.14}$$

The volume and surface integrals in Equations (2.10b,2.13) are computed using quadrature rules for tetrahedra and triangles, respectively (40; 15). The resulting matrix equation can be solved for the unknown magnetic flux density. In all the examples shown here, this equation is solved using a non-stationary iterative solver like (TF)QMR (35). If the material is linear, both the construction of the matrix equation and its solution are straightforward. Solving for fields in a non-linear media is a little more involved, and one needs to find a solution to the susceptibility iteratively. Before we proceed with the solution procedure, note that in Equations (2.11) and (2.14) apart from the permeability and susceptibility, the rest of the terms depend solely on the geometry. By virtue of the approximation that the permeability and the susceptibility are constant in each tetrahedron, these integrals can be precomputed and stored. The $\mathcal{Z}$ matrix can then be computed on the fly for each iteration that uses the

appropriate value of $\chi(\mathbf{r})$. The scheme for computing $\chi(\mathbf{r})$ proceeds as follows: (i) Start with an initial guess for $\chi^{(0)}(\mathbf{r})$; (ii) For any iteration i, compute the magnetic flux density by solving $\mathcal{Z}^{(i-1)}\mathcal{B}^{(i)} = \mathcal{H}$, where the superscript indicates that the results are obtained using the ith value of χ. As before an iterative solver like (TF)QMR is used together with a block-diagonal preconditioner; (iii) Use $\mathcal{B}^{(i)}$ to find $\chi^{(i)}(\mathbf{r})$ using either an approximate analytical model (12) or from a **B**–**H** curve; iterate until the prescribed convergence for $\chi(\mathbf{r})$ is reached using an appropriate non-linear solver. In most of the examples in this thesis, a globally convergent scheme like the Broyden's method (4) is used.

CHAPTER 3. ACCELARATION PROCEDURE

3.1 The Fast Multipole Method

It is apparent from the preceding description that the dominant cost of computing magnetic fields arises from computing the matrix vector product while using the iterative solver. Since $\mathcal{Z}$ is dense, using an iterative solver costs $\mathcal{O}(N^2)$ per iteration. Furthermore, another drawback is that the filling of $\mathcal{Z}$ is an $\mathcal{O}(N^2)$ process. These factors have in the past made integral equation based methods unattractive for practical analysis in spite of their many advantages. Fortunately, relieving this computational complexity was a topic of intense research (32; 28; 33; 23; 39; 7) over the past two decades. In the late eighties, Greengard and Rokhlin presented a seminal paper that discusses a multilevel fast algorithm for the N-body problem that considerably alleviates the computational complexity of computing kernels of the form $1/R$, where R is the distance between any two interacting pairs. It is apparent from the above equations that this method can be retrofitted into our codes to accelerate the matrix vector products.

In what follows, we present a gist of the scheme. Rigorous mathematical proofs regarding the validity and error bounds of this method can be found in (8). The FMM employs a divide and conquer strategy to accelerate field computation. This is achieved using a hierarchical subdivision of the body, which proceeds as follows: The body to be analyzed is enclosed in the fictitious cubical box. This box is recursively divided into eight boxes. A box that is subdivided into smaller boxes is termed the "parent" of the "child" boxes that have resulted from this operation. This systematic division leads to a uniform oct-tree structure. For an $n+1$-level scheme, this subdivision proceeds n times. At the lowest level, the boxes are populated by basis functions or equivalently a set of point magnetic dipoles and charges. The strengths of

these dipoles and charges can be trivially related to the quadrature rules used in Equations (2.13, 2.14). Potentials/fields due to these charges are computed at other locations by upward and downward traversal of the tree. In order to accomplish this in a hierarchical manner, the following dictum is used to create interaction lists: A pair of boxes at any level are said to be in the far field of each other if the distance between their centers is greater than a prescribed distance and if their parents are in the near field of each other. In practice, this distance, at any level, is chosen to be twice the linear dimension of the box at that level. Thus, for any given box at a level greater than one, interactions with boxes in the near field have to be resolved at lower levels in the tree. Interaction with a box in its far field can be computed at a higher level in the tree provided that the respective parent boxes are in the far field of each other. This concept of hierarchical ordering of computations is illustrated in Figure 3.1, depicted in two dimensions for clarity illustrates the hierarchical subdivision of a geometry placed in a fictitious cubical box and the interaction between the boxes at different levels. Also shown in the figure are the source blocks for an observer block for direct (i.e., near field) interaction, and interactions at level 1, 2 and 3. The matrix vector product required by the iterative solver is computed by first multiplying the vector with the sparse matrix that corresponds to interaction between the elements of level-1 boxes that are in the near-field of each other. All other contributions are computed using a top-down traversal.

3.2 Implementation of the FMM

The above description is intended to outline integration of the FMM within the classical solver. These ideas have been elaborated in great length in (8) and is hence, not repeated here. However, in implementing this algorithm several improvements some changes were made to that described in (8; 5), the principal of which is to exploit symmetry in the multipole coefficients. This reduces both the time and the memory required by the FMM portion by a factor of two.

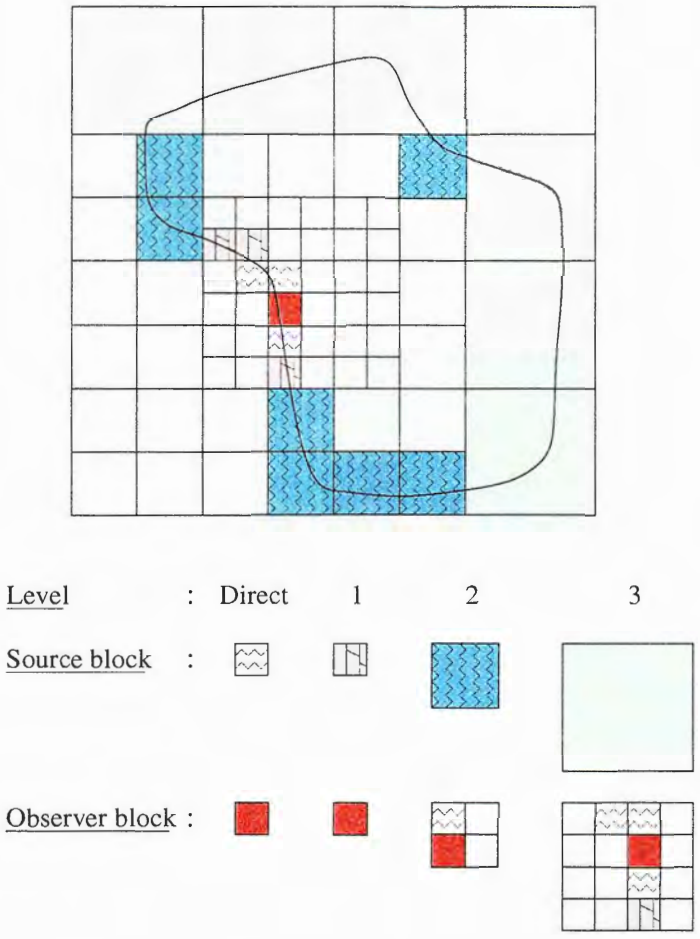

Figure 3.1 Interaction between boxes.

CHAPTER 4. RESULTS

4.1 Verification: Spherical Shell in a Uniform Field

This section presents numerous results that serve to verify the mathematical model and to confirm the applicability of the numerical procedure discussed thusfar while demonstrating the efficiency of the FMM augmented classical scheme.

As a first example, a linear problem for which exact analytical solutions are available is chosen. The numerically computed values for the magnetic scalar potential and the total magnetic field are compared against analytical solution to validate the above described numerical scheme. A spherical shell of inner radius a and outer radius b, made of material of permeability μ and placed in a uniform constant magnetic field $\mathbf{B}_o$ $(= B_o\hat{z})$ is considered (see Figure 4.1). The analytical expressions for the scalar potential and the total magnetic fields at any point $(r, \theta, 0)$ are given by (13) as

$$\phi^p(r,\theta,0) = \begin{cases} \dfrac{\alpha}{\mu_0 r^2}\cos(\theta) & r > b \\ \dfrac{1}{\mu_0}(\delta r\cos(\theta) + B_0 r\cos(\theta)) & r < a \end{cases} \tag{4.1a}$$

$$H_r^t(r,\theta,0) = \begin{cases} \dfrac{1}{\mu_0}(B_0\cos(\theta) + \dfrac{2\alpha}{r^3}\cos(\theta)) & r > b \\ -\dfrac{1}{\mu_0}\delta\cos(\theta) & r < a \end{cases} \tag{4.1b}$$

$$H_\theta^t(r,\theta,0) = \begin{cases} \dfrac{1}{\mu_0}(-B_0\sin(\theta) + \dfrac{\alpha}{r^3}\sin(\theta)) & r > b \\ \dfrac{1}{\mu_0}\delta\sin(\theta) & r < a \end{cases} \tag{4.1c}$$

where

$$\alpha = \left[\frac{(2\mu+1)(\mu-1)}{(2\mu+1)(\mu+2) - 2\frac{a^3}{b^3}(\mu-1)^2} \right] (b^3 - a^3)B_0 \tag{4.1d}$$

and

$$\delta = \left[\frac{9\mu}{(2\mu+1)(\mu+2) - 2\frac{a^3}{b^3}(\mu-1)^2} \right] B_0 \tag{4.1e}$$

In our experiment, a spherical shell of outer radius 3.5 meters and inner radius 2.0 meters was discretized into 468 tetrahedral elements, and B_0 was chosen to be $4\pi \times 10^{-7}$ T. The total magnetic field and the scalar potential were computed both inside and outside the shell for different values of the permeability. Figures 4.2 and 4.3 compare the results obtained numerically and analytically at a radius of 5m for $\mu_r = 2$ and $\mu_r = 1000$, respectively. Figures 4.4 and 4.5 compare the analytical and numerical results at a radius of 0.5m for $\mu_r = 2.0$ and $\mu_r = 1000$. The analytical and numerical results presented in Figures 4.2–4.5 indicate the accuracy of the prescribed method. In our analysis, excellent agreement was observed between the analytical solutions and numerical results for a wide range of μ_r and radii of observation.

4.2 Coil Surrounding a Ferromagnetic Material

As a second example, the practical problem of magnetic flux leakage (MFL) inspection used in nondestructive testing (22; 21) is considered. In this application, a ferromagnetic sample to be analyzed is first magnetized. Cracks in the sample produce leakage flux in air surrounding the sample. The detection of leakage flux is indicative of defects in the material. The sample can be magnetized by a coil or by another magnet. In our experiments, a nonlinear material in the shape of a cylinder was chosen as shown in Figure 4.6. The material has a radius of 50 mm and a height of 30 mm and is placed so that its axis coincides with the Z axis. It is surrounded by a coil with inner and outer radii 55 mm and 60 mm respectively and is 10 mm thick. This problem was modeled using a geometry consisting of 314 tetrahedrons. The nonlinearity of the material is characterized by the **B-H** curve shown in Figure 4.7. The coil

was excited by a current of 5000 A and the flux density due to the sample was observed at various loacations in air on the $y = 0$ plane. Figure 4.8 is a contour plot of absolute values of the flux density due to the material, B_r and B_z, on the $X - Z$ plane, in the absence of any defect.

A defect was created in the cylinder by removing a portion of the cylinder in the shape of a pillbox of size 1mm $\times$ 1mm $\times$ 1mm. This defect was located on the wall of the cylinder, symmetric about the positive X axis. Figure 4.9 is a contour plot of the absolute values of B_r and B_z, on the $X - Z$ plane, with this defect. Figures 4.10 and 4.11 are the contour plots for defects of sizes 2mm $\times$ 2mm $\times$ 2mm and 4mm $\times$ 4mm $\times$ 4mm respectively.

4.3 Team Problem 13

Next the benchmark Problem 13 defined in the TEAM Workshop (26) is considered. The Team Problem 13, (refer Figure 4.12), consists of two steel channels with a steel plate inserted between the channels. A coil is set between two steel channels and is excited by a DC current of 1000 AT. The nonlinearity is modeled by the **B**–**H** curve shown in Figure 4.13. The curve for high flux densities ($|\mathbf{B}| \geq 1.8T$) is approximated by the following equations:

$$B = \begin{cases} \mu_0 H + (aH^2 + bH + c) & (1.8 \leq B \leq 2.22T) \\ \mu_0 H + Ms & (B \geq 2.22T) \end{cases} \tag{4.2}$$

where the constants a, b and c are -2.822×10^{-10}, 2.529×10^{-5} and 1.591, respectively. Ms is the saturation magnetization (2.16T) of the steel. The objective is to compute the magnetic fields at various positions. The problem was discretized into 18293 tetrahedral elements with 43195 unknowns. Due to the geometry of the problem, the interaction matrix ($\mathcal{Z}$) becomes highly ill-conditioned thereby affecting convergence rate of the TFQMR. For faster convergence, a block diagonal preconditioner was used in conjunction with TFQMR. The values of the average flux densities obtained numerically are plotted against measured values for comparison (Figure 4.14). Figure 4.15 shows a normalized surface plot of the distribution of magnetic flux density on the plates.

4.4 Computational Complexity

Finally, the theoretically predicted scaling laws for both complexity and memory requirements are experimentally verified. The results are obtained on a 500 MHz Linux PC. In Figure 4.16(a), the logarithm of computational time required for both the classical and FMM augmented solvers are plotted against the logarithm of the number of unknowns. It can be verified that the slopes for the direct and FMM augmented schemes are 1.998 and 1.013, respectively. The break-even point is around 300 unknowns. Likewise, Figure 4.16(b) compares the memory requirements of the classical and FMM augmented schemes. Again the breakeven point is around 250 unknowns. These results were obtained for an accuracy of 10^{-3}; the accuracy dictates the number of multipoles and associated integration rules.

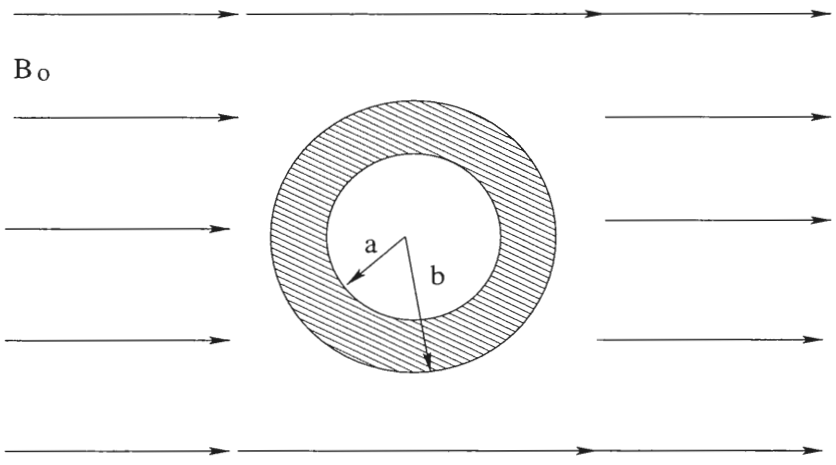

Figure 4.1 Spherical Shell in a uniform field.

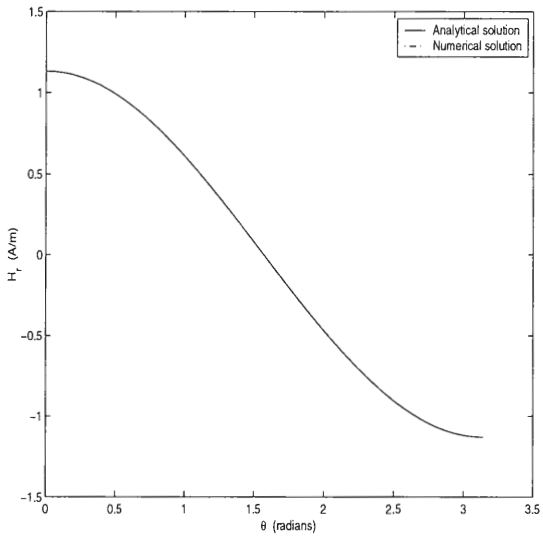

(a) Plot of H_r

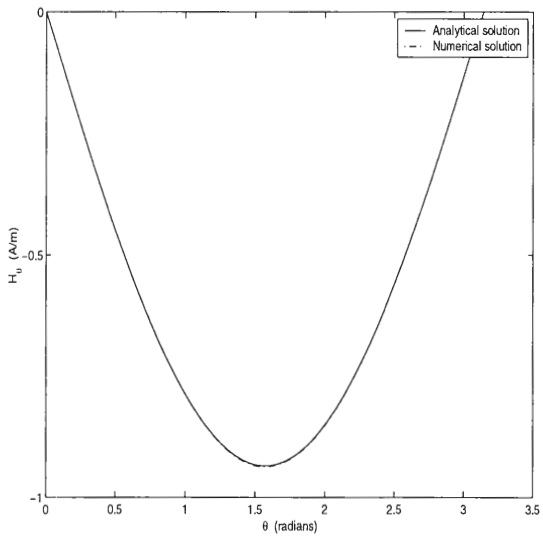

(b) Plot of H_θ.

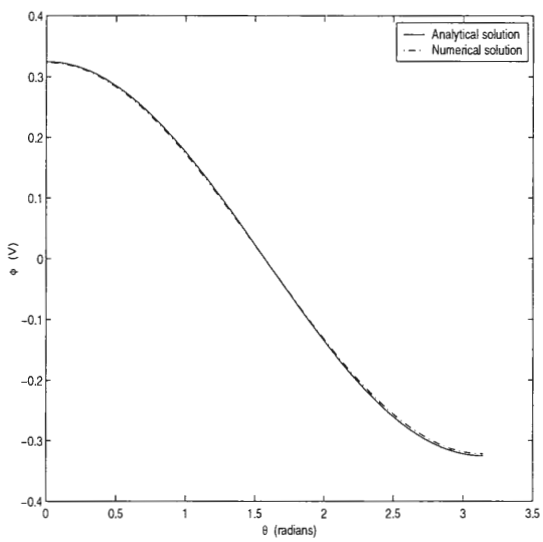

(c) Plot of ϕ.

Figure 4.2 Spherical Shell with $r = 5$ meters and $\mu_r = 2.0$.

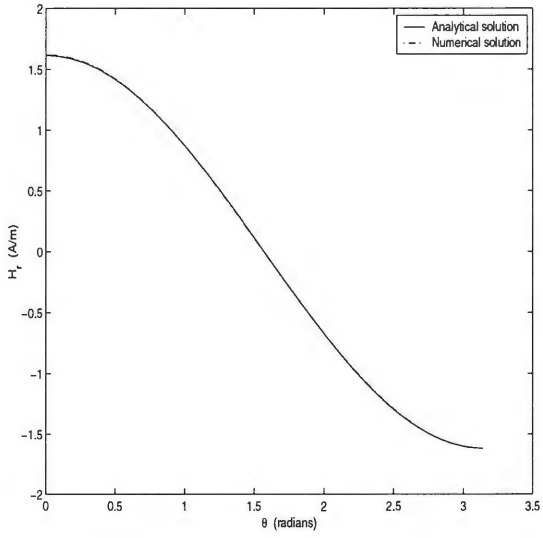

(a) Plot of H_r

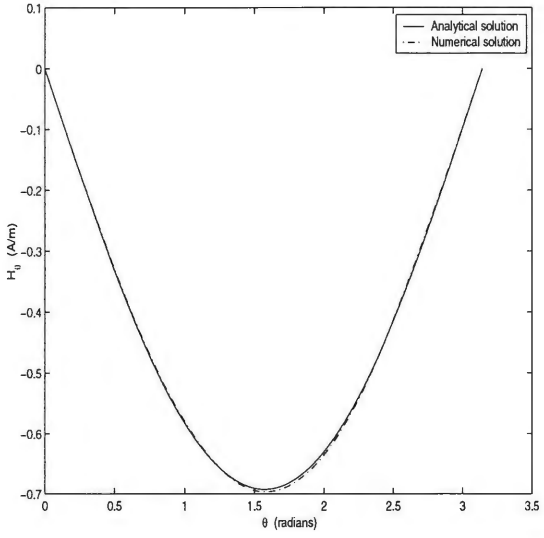

(b) Plot of H_θ.

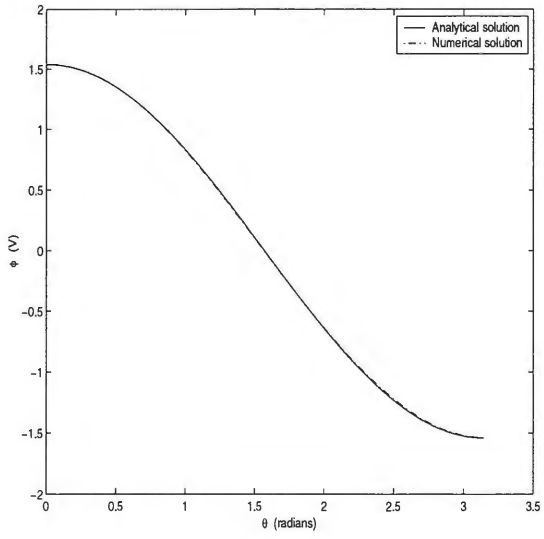

(c) Plot of ϕ.

Figure 4.3 Spherical Shell with $r = 5$ meters and $\mu_r = 1000.0$.

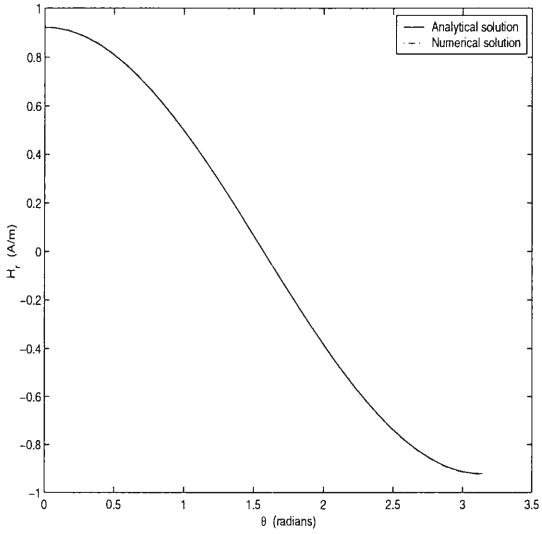

(a) Plot of H_r

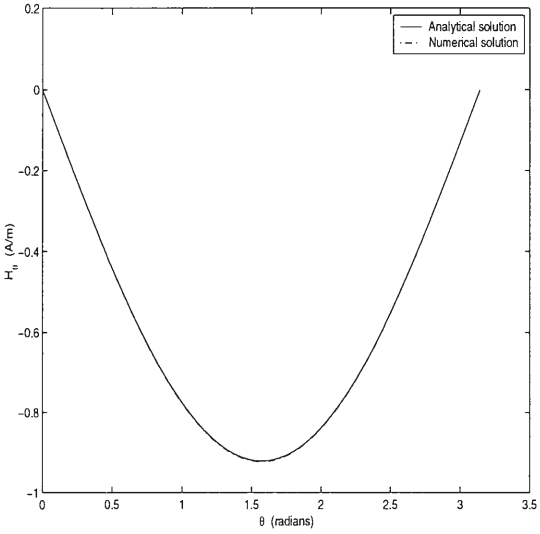

(b) Plot of H_θ.

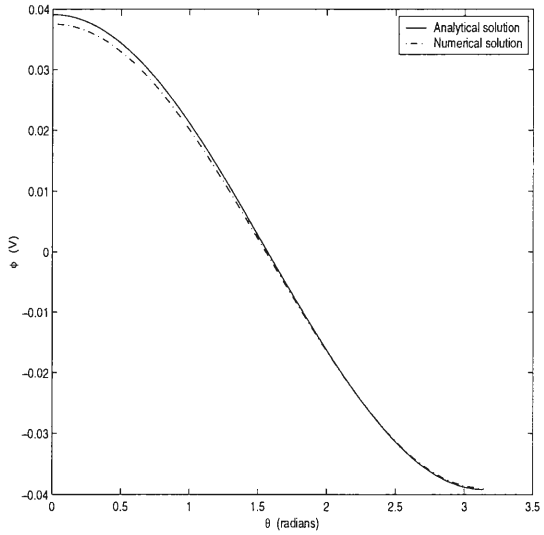

(c) Plot of ϕ.

Figure 4.4 Spherical Shell with $r = 0.5$ meters and $\mu_r = 2.0$.

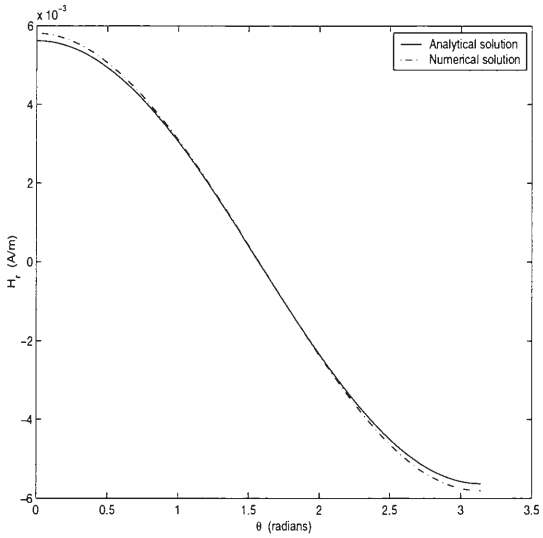

(a) Plot of H_r

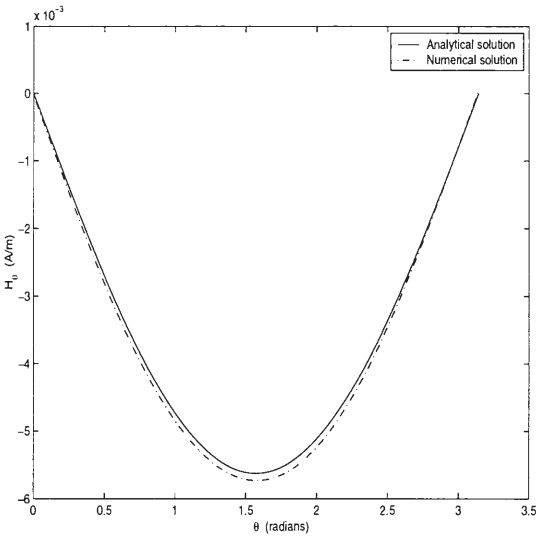

(b) Plot of H_θ.

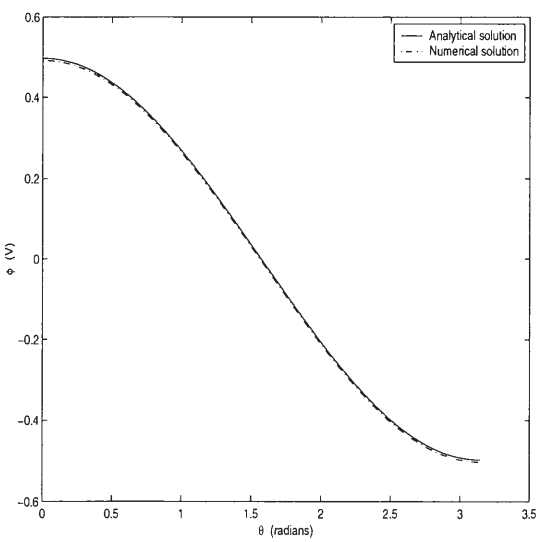

(c) Plot of ϕ.

Figure 4.5 Spherical Shell with $r = 0.5$ meters and $\mu_r = 1000.0$.

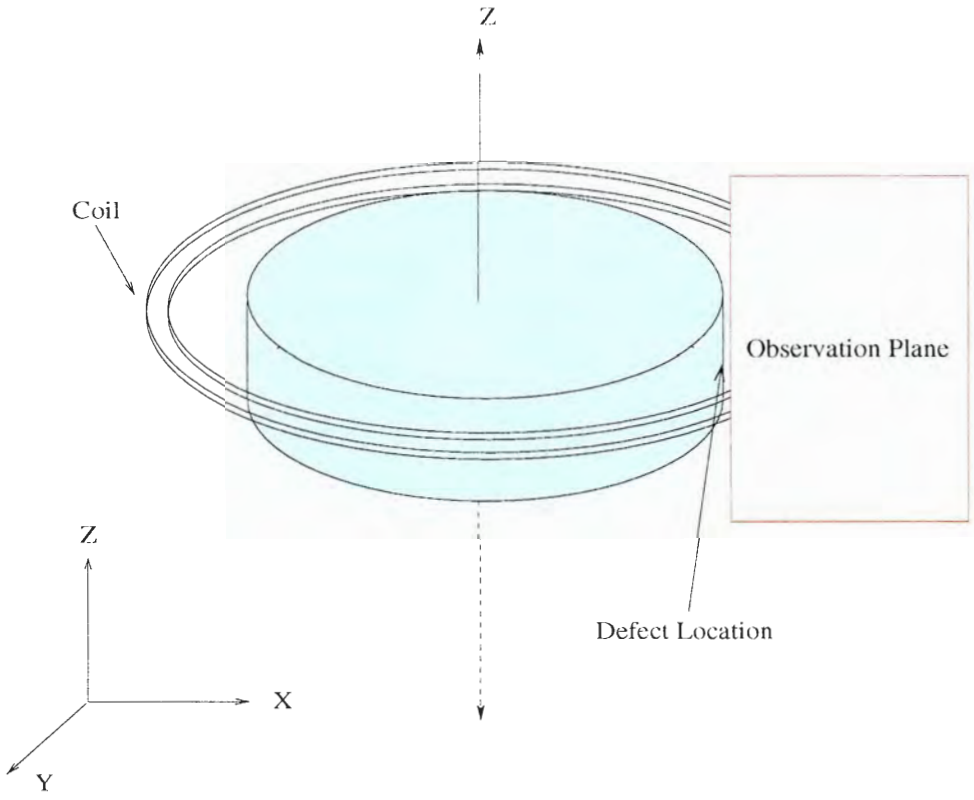

Figure 4.6 Coil Surrounding a Ferromagnetic Material.

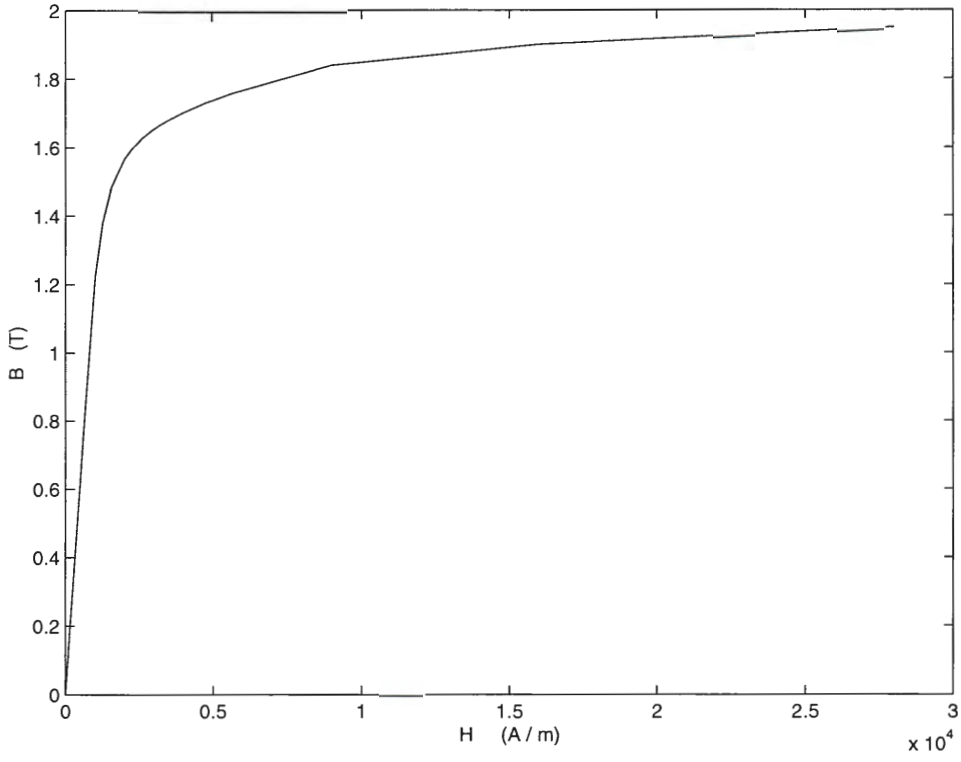

Figure 4.7 **B-H** curve of steel.

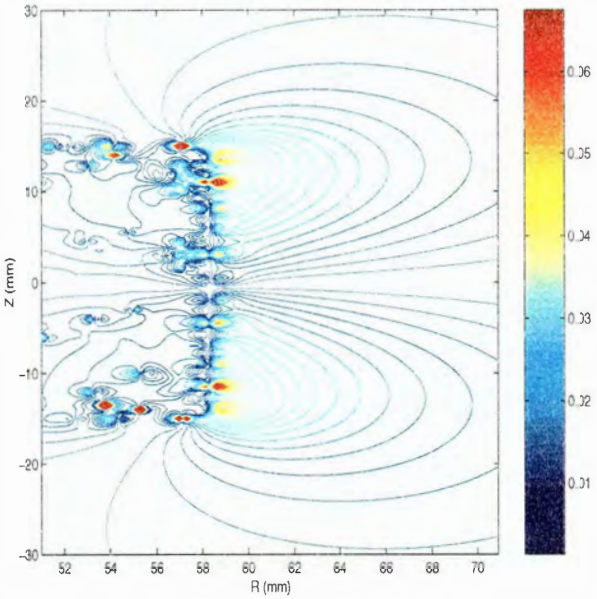

(a) Contour Plot of $|B_r|$.

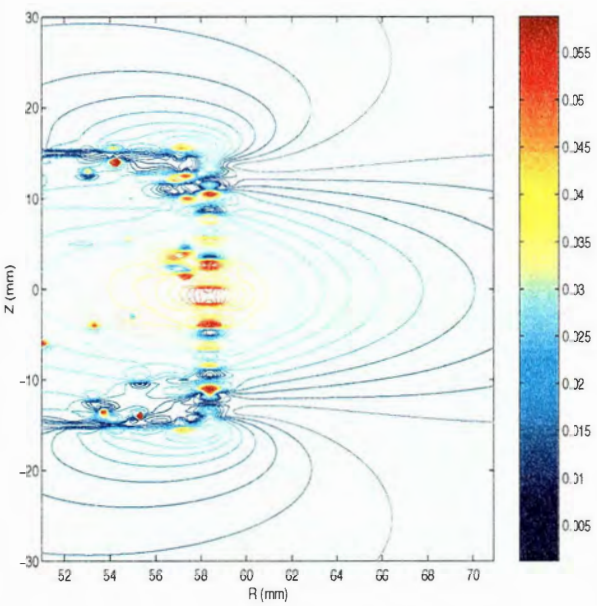

(b) Contour Plot of $|B_z|$.

Figure 4.8 Defect-free cylinder.

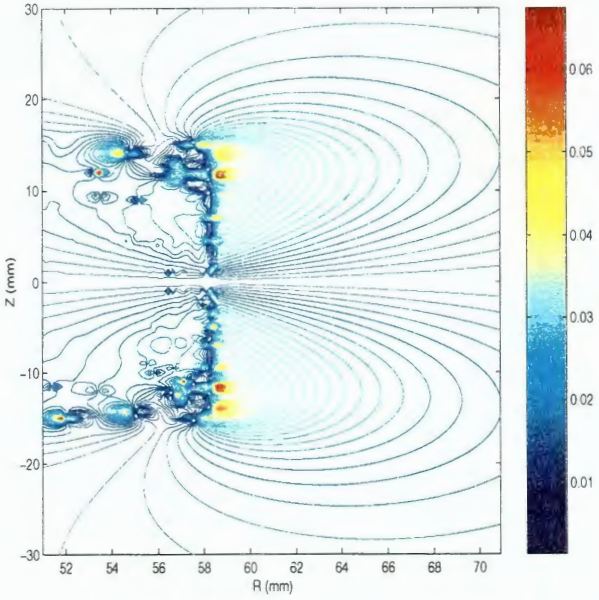

(a) Contour Plot of $|B_r|$.

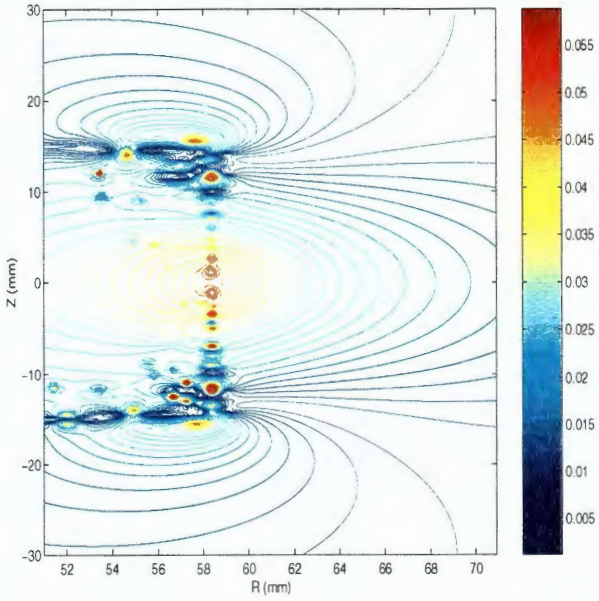

(b) Contour Plot of $|B_z|$.

Figure 4.9 Cylinder with a defect sized 1mm × 1mm × 1mm.

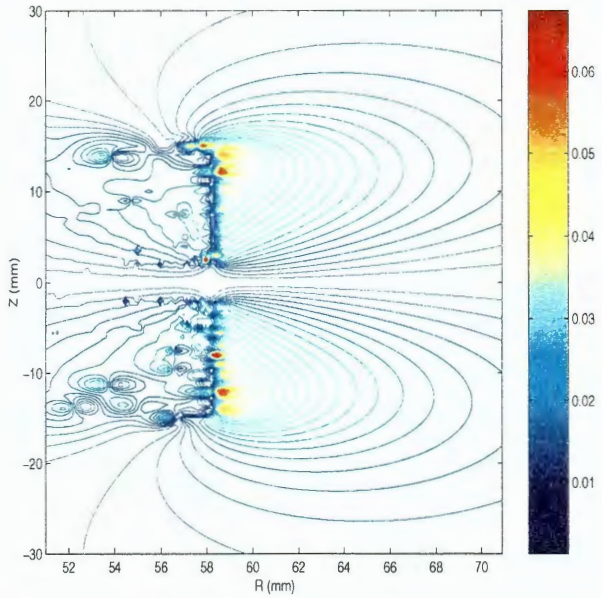

(a) Contour Plot of $|B_r|$.

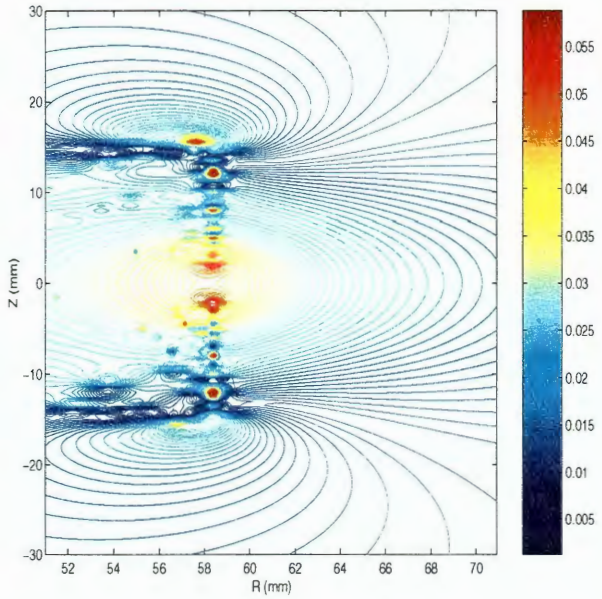

(b) Contour Plot of $|B_z|$.

Figure 4.10 Cylinder with a defect sized 2mm × 2mm × 2mm.

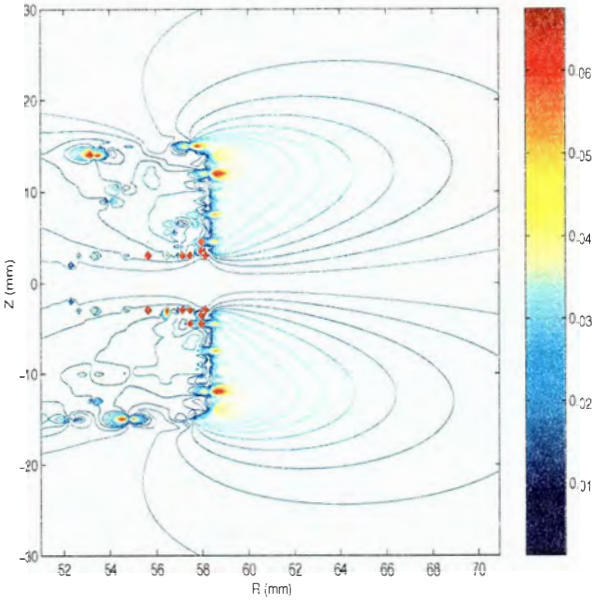

(a) Contour Plot of $|B_r|$.

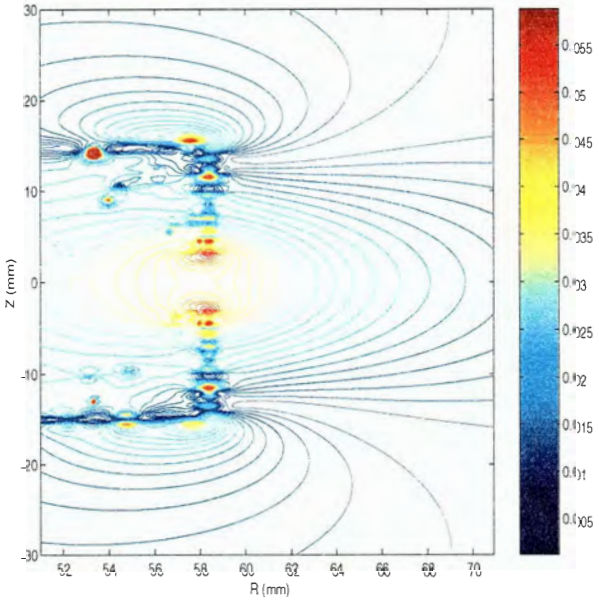

(b) Contour Plot of $|B_z|$.

Figure 4.11 Cylinder with a defect sized 4mm × 4mm × 4mm.

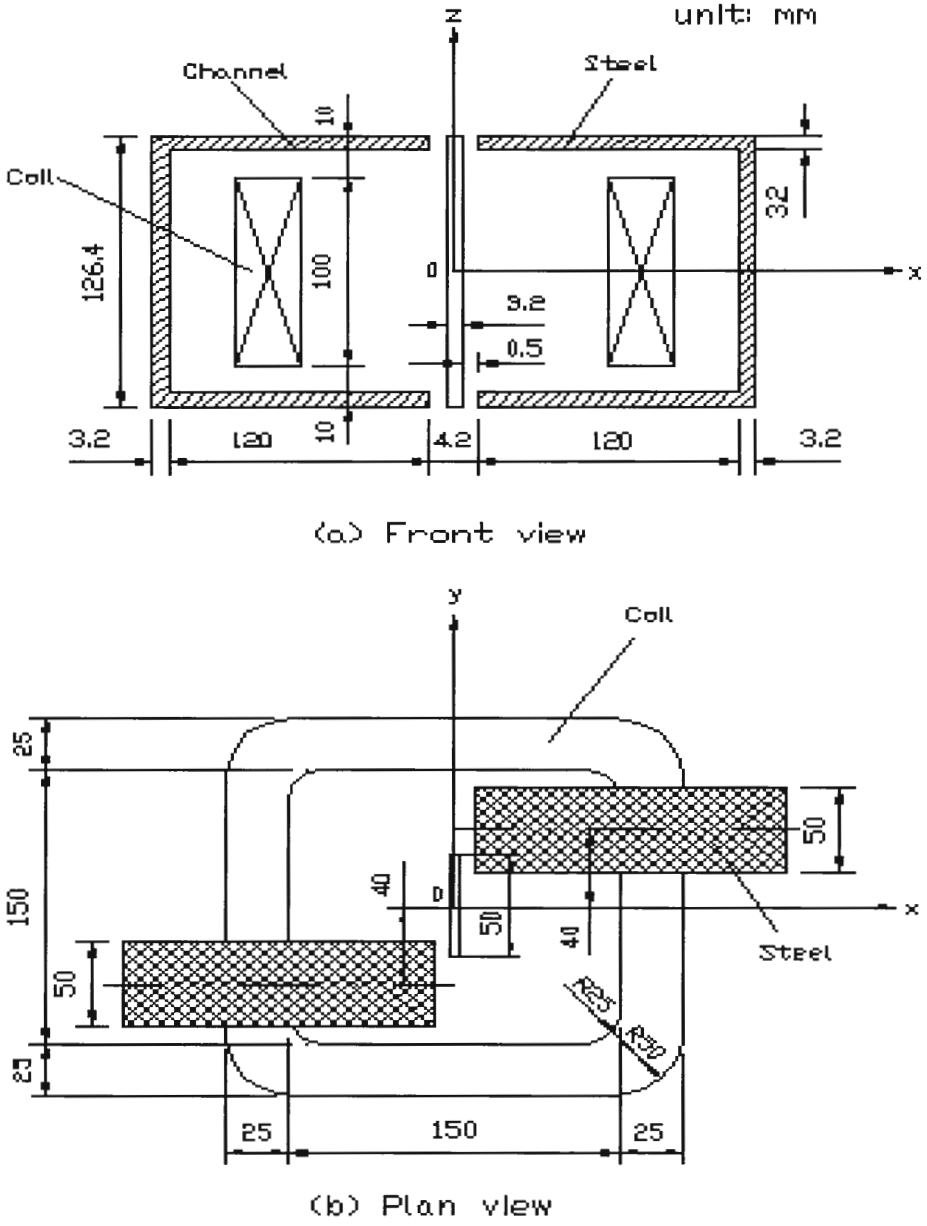

Figure 4.12 TEAM Problem 13.

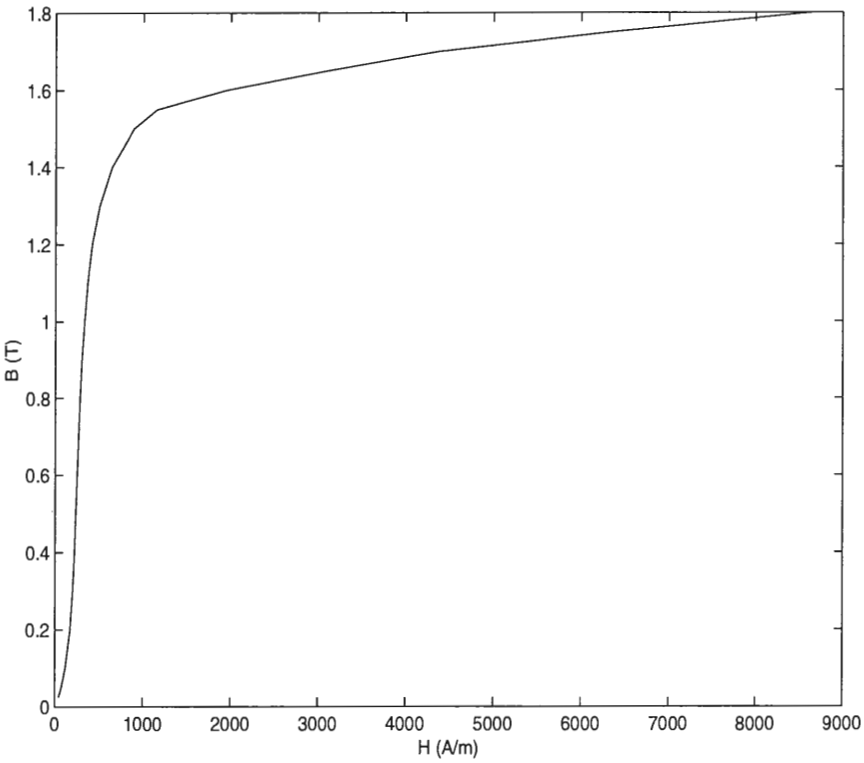

Figure 4.13 **B**–**H** curve for TEAM Problem 13.

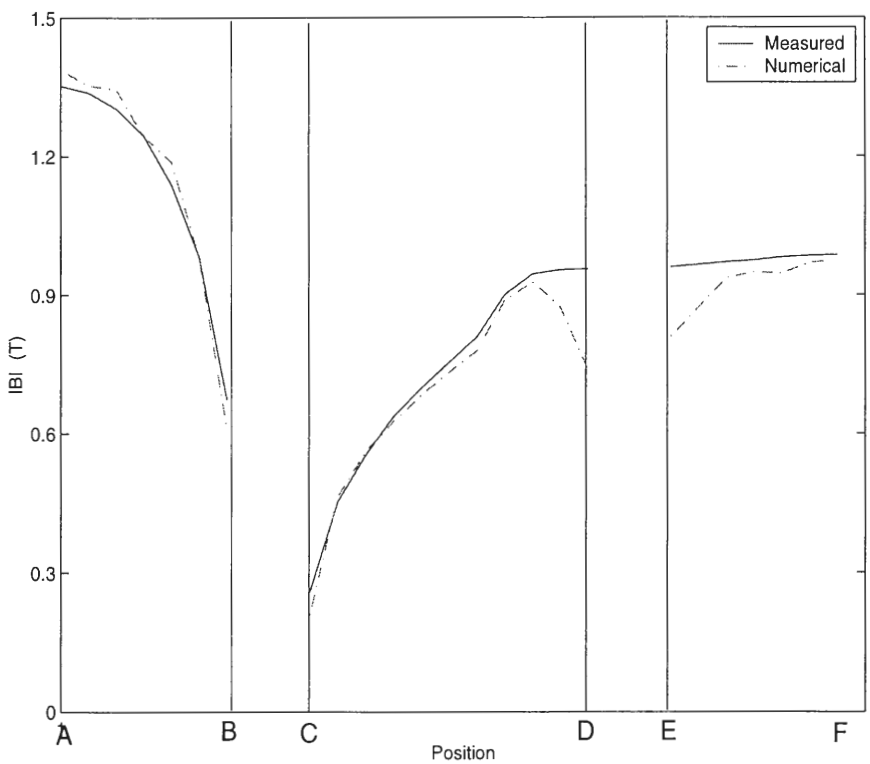

Figure 4.14 Distribution of average magnetic flux density in the steel plates.

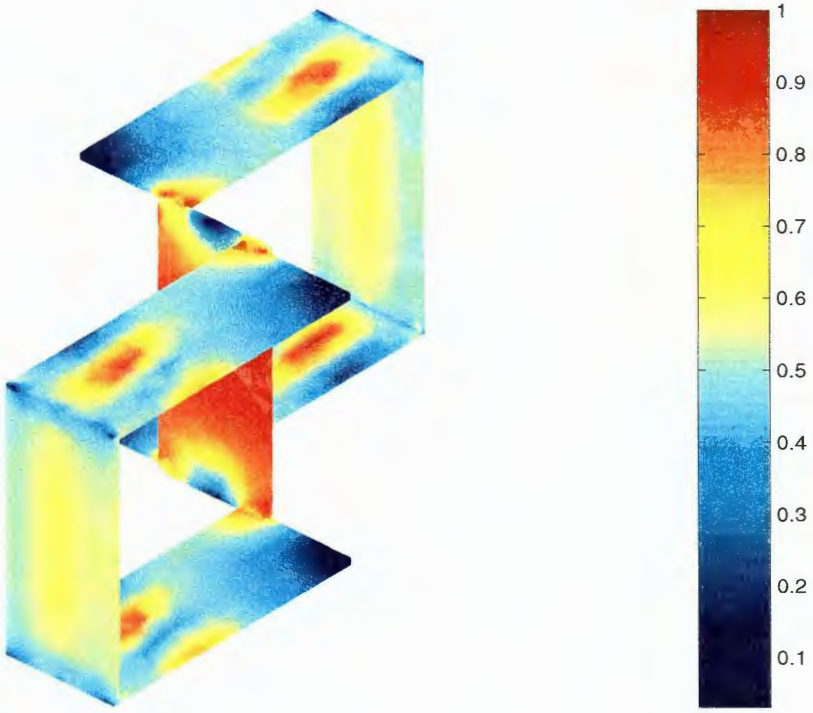

Figure 4.15 Surface plot of the flux distribution in the steel plates (normalized).

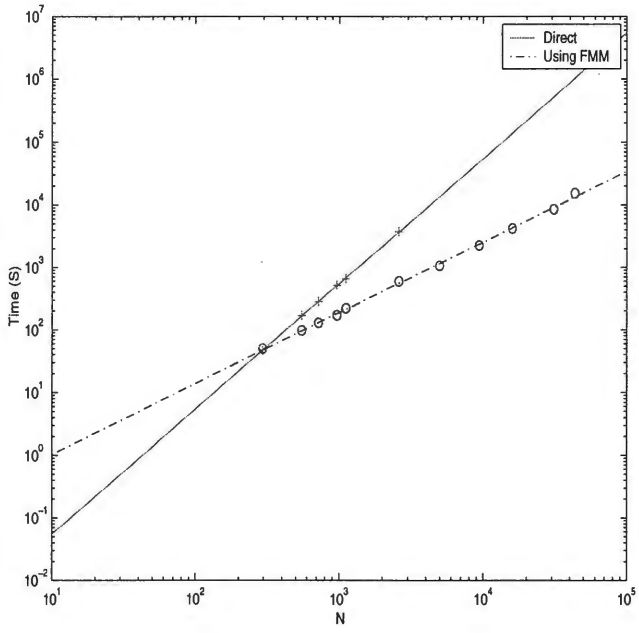

(a) CPU Times.

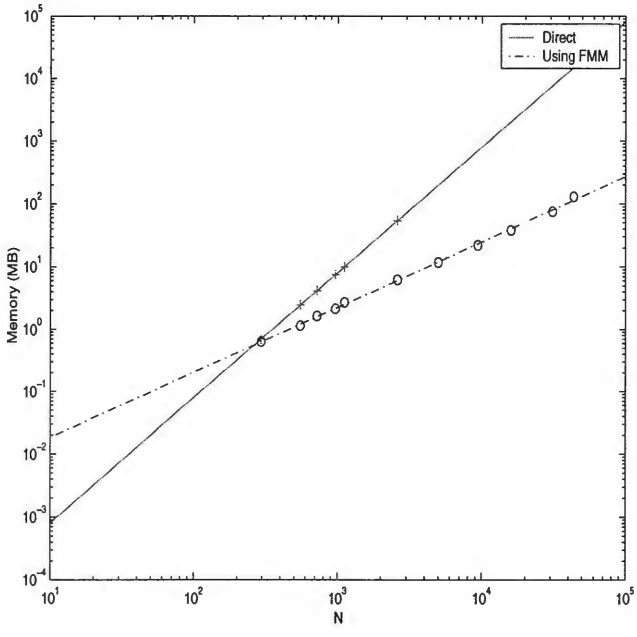

(b) Memory.

Figure 4.16 Computational complexity.

CHAPTER 5. CONCLUSION

This thesis presented a novel integral equation for solving nonlinear magneto-static problems. The integral equation has been solved using the classical solver that is augmented with FMM. Numerical simulations that were conducted demonstrate the accuracy and usefulness of the prescribed formulation.

APPENDIX COMPUTATION OF ROTATION COEFFICIENTS

In this section, formulae for the evaluation of the rotation coefficients for spherical harmonics are expressed in terms of the binomial coefficents. Suppose that $Y_n^m(\theta,\phi)$ are the spherical harmonics of a point (r,θ,ϕ) in the original coordinate system and that α,β and γ are the Eulerian angles (refer (6), (9)). The spherical harmonics under rotation are transformed by

$$Y_n^m(\theta',\phi') = \sum_{m'=-l}^{l} G_{m'm}^n(\alpha\beta\gamma) Y_n^{m'}(\theta,\phi) \tag{A.1}$$

where (θ',ϕ') is the spherical angular coordinate of the point after rotation in the original coordinate system and $G_{mm'}^n(\alpha\beta\gamma)$ are the rotation coefficients to be computed. For the rotation of complex spherical harmonics, the rotation coefficients are defined by the formula (9),

$$G_{m'm}^n(\alpha\beta\gamma) = e^{-im'\alpha - im\gamma} d_{m'm}^l(\beta) \tag{A.2}$$

where

$$d_{m'm}^l(\beta) = K \sum_{\gamma=0}^{j-m'} \begin{pmatrix} j-m \\ \gamma \end{pmatrix} \begin{pmatrix} j+m \\ j-m'-\gamma \end{pmatrix} (\sin\frac{\beta}{2})^{2j-(2\gamma-m'+m)} (\cos\frac{\beta}{2})^{2\gamma-m'+m} \tag{A.3}$$

where

$$K = \left[\frac{(j+m')!(j-m')!}{(j+m)!(j-m)!}\right]^{\frac{1}{2}} \tag{A.4}$$

Additional materials on the definition of Eulerian angles and the derivation of rotation coefficients can be found in references (1) and (6).

BIBLIOGRAPHY

[1] L. C. Biedenharn and J. D. Louck. *Angular Momentum in Quantum Physics: Theory and Application.* Addison Wesley, Reading, MA., 1981.

[2] J. A. Board, J. W. Causey, J. F. Leathrum, A. Windemuth, and K. Schulten. Accelerated molecular dynamics with the fast multipole algorithm. *Chemical Physics Letters*, 198(1):89–94, October 1992.

[3] J. R. Bowler and N. Harfield. Magnetic field evaluation for application to magnetic particle inspection. In *The Fifth International Workshop on Electromagnetic Non Destructive Evaluation*, August 1999.

[4] C. G. Broyden. A class of methods for solving nonlinear simultaneous equations. *Mathematics of Computation*, 19(92):577–593, October 1965.

[5] H. Cheng, L Greengard, and V Rokhlin. A fast adaptive multipole algorithm in three dimensions. *Journal of Computational Physics*, 155:468–498, 1999.

[6] A. R. Edmonds. *Angular Momentum in Quantum Mechanics.* Princeton University Press, Princeton, New Jersey, 1957.

[7] H. Fujiwara. The fast multipole method for integral equations of seismic scattering problems. *Geophysical journal international*, 133(3):773–782, June 1998.

[8] L. Greengard and V. Rokhlin. A new version of the fast multipole method for the laplace equation in three dimensions. *Acta Numerica*, pages 229–269, 1997.

[9] I.I. Guseinov. On the evaluation of rotation coefficients for spherical harmonics using binomial coefficients. *Journal of Molecular Structure*, 366:119–121, 1996.

[10] L. Han, L. Tong, and J. Yang. Integral equation method using total scalar potential for the simulation of linear or nonlinear 3d magnetostatic field with open boundary. *IEEE Trans. on Magnetics*, 30(5):2897 –2900, September 1994.

[11] R. F. Harrington. *Field Computation by Moment Methods.* Macmillan, NewYork, 1968.

[12] A. Ivanyi. *Hysteresis Models In Electromagnetic Computation.* Akademiai Kiado, Budapest, 1997.

[13] J. D. Jackson. *Classical Electrodynamics.* John Wiley and Sons, NewYork, 1975.

[14] N. Katz and S. White. Hierarchical galaxy formation: overmerging and the formation of an x-ray cluster. *Astrophysical Journal*, 412:412 – 455,, 1993.

[15] P. Keast. Moderate-degree tetrahedral quadrature formulas. *Computer Meth. Appl. Mechanics Eng.*, 55:339–348, 1986.

[16] L. Kettunen, K. Forsman, D. Levine, and W. Gropp. Volume integral equations in nonlinear 3d magnetostatics. *International journal of numerical methods in engineering*, 38:2655–2675, 1995.

[17] S. Kikuchi and H. Kimura. Some considerations on the magnetic shielding in the train. *IEEE Trans. on Magnetics*, 31(6):4256–4258, November 1995.

[18] M. Koizumi, M. Onisawa, and M Utamura. Three dimensional magnetic field analysis method using scalar potential formulated by boundary element method. *IEEE Trans. on Magnetics*, 26(2):360–363, March 1990.

[19] B. Krstajic, Z. Andelic, S. Milojkovic, S. Babic, and S. Salon. Nonlinear 3d magnetostatic field calculation by the integral equation method with surface and volume magnetic charges. *IEEE Trans. on Magnetics*, 28(2):1088–1091, March 1992.

[20] D. Levine, W. Gropp, K. Forsman, and L. Kettunen. Parallel computation of three-dimensional nonlinear magnetostatic problems. *Concurrency: Practice and Experience*, 11(2):109–120, 1999.

[21] W. Lord and J. H. Hwang. Defect characterization from magnetic leakage fields. *The British Journal of Nondestructive Testing*, 19(1):14, January 1977.

[22] W. Lord and D. J. Oswald. Leakage methods of field detection. *International Journal of Nondestructive Testing*, 4(3):249–274, December 1972.

[23] C. C. Lu and W. C. Chew. Fast algorithm for solving hybrid integral equations. *IEE Proceedings-H*, 140(6):455–560, December 1993.

[24] M. Marinescu and N. Marinescu. Magnetic leakage fields from extended inhomogeneities in ferromagnetic plates. *IEEE Trans. on Magnetics*, 30(5):2960–2963, September 1994.

[25] K Nabors and J White. Fastcap: a multipole accelerated 3-d capacitance extraction program. *IEEE Transactions on Computer-Aided Design of Integrated Circuits and Systems*, 10(11):1447–1459, November 1991.

[26] T. Nakata, N. Takahashi, K. Fujiwara, K. Muramatsu, T. Imai, and Y. Shiraki. Numerical analysis and experiments of 3-d non-linear magnetostatic model. In *Proc. Int. Symp. and TEAM Workshop*, volume 9, Supplement A, pages 308–310, Okayama, Japan, 1990.

[27] M. J. Newman, C. W. Trowbridge, and L. R. Turner. Gfun: An interactive program as an aid to magnet design. In *Proc. 4th Int. Conf. Magn. Tech.*, Brookhaven, New York, September 1972.

[28] S. T. O'Donnell and V. Rokhlin. A fast algorithm for the numerical evaluation of conformal mappings. *SIAM Journal on Scientific and Statistical Computing*, 10(3):475–487, May 1989.

[29] K. Preis, I. Bardi, O. Biro, C. Magele, W. Renhart, K. R. Richter, and G. Vrisk. Numerical analysis of 3d magnetostatic fields. *IEEE Trans. on Magnetics*, 27(5):3798 –3803, September 1991.

[30] S. M. Rao, D. R. Wilton, and A. W. Glisson. Electromagnetic scattering by surfaces of arbitrary shape. *IEEE Trans. on Antennas and Propagation*, 30(3):409–418, May 1982.

[31] J. R. Reitz and F. J. Milford. *Foundations of Electromagnetic Theory.* Addison-Wesley Publishing Company, Inc., Reading, Massachusetts, USA, 1960.

[32] V. Rokhlin. Rapid solution of integral equations of classical potential theory. *Journal of Computational Physics*, 60:187–207, 1985.

[33] V. Rokhlin. Rapid solution of integral equations of scattering theory in two dimensions. *Journal of Computational Physics*, 86(2):414–439, February 1990.

[34] W. M. Rucker, Ch. Magele, E. Schlemmer, and K. R. Richter. Boundary element analysis of 3-d magnetostatic problems using scalar potentials. *IEEE Trans. on Magnetics*, 28(2):1099–1102, March 1992.

[35] Y. Saad. *Iterative methods for sparse linear systems.* PWS series in computer science. PWS Pub. Co., Boston, 1996.

[36] D. H. Schaubert, D. R. Wilton, and A. W. Glisson. A tetrahedral modeling method for electromagnetic scattering by arbitrarily shaped inhomogeneous dielectric bodies. *IEEE Trans. on Antennas and Propagation*, 32(1):77–85, January 1984.

[37] J. Simkin. A comparison of integral and differential equation solutions for field problems. *IEEE Trans. on Magnetics*, 18(2):401–405, 1982.

[38] J. Simkin and C. W. Trowbridge. On the use of total scalar potential in the numerical solution of field problems in electromagnetics. *International journal of numerical methods in engineering*, 14(3):423–440, 1979.

[39] J. M. Song and W. C. Chew. Fast multipole method solution of three dimensional integral equation. In IEEE, editor, *IEEE Antennas and Propagation Society International Symposium: 1995 digest, June 18–June 23, 1995, Newport Beach, California*, volume 2–3, pages 1528–1531, 1109 Spring Street, Suite 300, Silver Spring, MD 20910, USA, 1995. IEEE Computer Society Press. Four volumes. IEEE catalog number: 95CH35814.

[40] K. S. Sunder and R. A. Cookson. Integration points for triangles and tetrahedrons abtained from the gaussian quadrature points for a line. *Computers and Structures*, 21(5):881–885, 1985.

[41] C. W. Trowbridge. Electromagnetic computing: The way ahead? *IEEE Trans. on Magnetics*, 24(1):13–18, January 1988.

[42] K. Urata and A. Kameari. Static magnetic field analyses by integral method using magnetization with normal continuity in shell structure. *IEEE Trans. on Magnetics*, 31(3):1440–1443, May 1995.

[43] Y. Xiao and Y. Lu. The hybrid perfectly matched layer and finite element solution for open region problems. *IEEE Trans. on Magnetics*, 36(4):1635 –1639, July 2000.

ACKNOWLEDGEMENTS

I would like to take this opportunity to express my thanks to those who helped me with various aspects of conducting research and the writing of this thesis. First and foremost, Dr. Shanker Balasubramanian for his guidance, patience and support throughout this research and the writing of this thesis. His insights and words of encouragement have often inspired me and renewed my hopes for completing my graduate education. I would also like to thank my committee members for their efforts and contributions to this work: Dr. Lalita Udpa, Dr. Satish S. Udpa and Dr. Paul Sacks.